First Place Tie 2001 Roon Awards Competition

Interaction of Rheology, Geometry, And Process in Coating Flow

Richard R. Eley—ICI Paints*
Leonard W. Schwartz—University of Delaware†

A final coating of uniform thickness implies good leveling and the avoidance of defects during film formation. Though generally desired, this objective is often unmet. The outcome of a coating process depends on the nonlinear interaction of the rheology, process variables, and substrate geometry. Understanding the role of rheology is complicated by difficulties in linking fundamental rheological properties with coating performance. During a coating process, forces of varying type, magnitude and duration act on the fluid film. For non-Newtonian coatings the viscosity varies with both time and position within the coating layer, making predictions of flow behavior quite difficult. One answer is computer simulation, using numerical techniques to solve a set of nonlinear differential equations governing the flow. The rheological and other physical properties are parameter values for the program.

We present results of mathematical modeling and numerical simulation of a coating imperfection known as a "dripmark." The model includes non-Newtonian rheology, substrate shape, surface tension, and gravity. We compare theoretical prediction with experimental observation in a study of two architectural paints. We also describe a new method of quantitatively measuring the surface profile of a coating defect.

INTRODUCTION

Rheology and Coating Flows

One of the unsolved problems of the protective and decorative coatings industry is how to understand the relationship of rheology to coating flows. As stated by Strivens,[1] "Both the theory and the experimental evidence provided to understand paint flow will appear sketchy . . . in many areas." It is well accepted that rheology governs the application behavior and the post-application flow of a coating layer. However, it is still far from clear how knowledge of the fundamental rheological properties can be used to control specific details of product performance. The link between measured fundamental properties and real-world performance is still a weak one. One reason is that coating flows are really quite complex. The majority of paints and coatings are non-Newtonian, which makes it difficult to estimate the governing viscosity for a given coating process. In fact, the viscosity of a non-Newtonian coating can vary with both time and position within a coater or applicator device, as well as within a liquid layer during post-application flow and film formation. For example, for gravity-driven sagging or drainage flow, the maximum shear stress is at the coating-substrate interface, and in a loose sense is equal to the "weight" of the paint layer from there to the free surface. That shear stress is calculable, and one can obtain a single viscosity controlling sagging at that shear stress from a flow curve. However, one must remember that the gravitational shear stress will vary through the coating layer, from a maximum value at the substrate to zero at the free surface. The viscosity likewise varies inversely (and nonlinearly) through the coating layer. Therefore, the exact sagging behavior must be calculated as a *flux*, the integral of the velocity through the thickness of the film, mediated by the non-Newtonian viscosity function. (See equations (7) and (9).)

Generally, a prime success criterion for coatings is the achievement of a uniform layer as the outcome of the film formation and solidification process. A final film of uniform thickness implies good flow and leveling and the

Presented at the 79th Annual Meeting of the Federation of Societies for Coatings Technology, on Nov. 3-5, 2001, in Atlanta, GA.
*Strongsville Research Center, 16651 Sprague Rd., Strongsville, OH 44136.
†Dept. of Mechanical Engineering, University of Delaware, Newark, DE 19716.

avoidance of undesired flows in the course of film formation. Achievement of this goal is complicated by complex rheology, substrate irregularities, geometric and rate factors involved in the application process, surface tension gradients, and environmental factors. The precise outcome of a coating process depends on the detailed, nonlinear interplay of the rheology, process details, and substrate geometry. Occasionally, the result is a coating defect of the type that can be described as an undesired flow.

One answer to the complexity of coating processes is computer simulation, in which the fundamental rheological data become parameter values for the model. Computerized numerical techniques are used to solve a set of nonlinear differential equations that govern the flow. A complete model should take account not only of coating rheological and other physical properties but also of process details, complexities of substrate geometry, ambient environmental factors, and changes in properties with evaporation and temperature. A model containing the correct physics affords a detailed understanding of coating processes, the use of computer simulation as a surrogate for wet experiments, and the ability to explore and optimize the interrelationship of rheology and processes.

Rheology and Coating Flow Defects

Coatings can be afflicted by many kinds of imperfections or defects, which challenge the resourcefulness of practitioners from formulator to end-user. The correction and control of defects, therefore, is an ongoing task for the industry. Schoff[2] and others[3,4] have reviewed the causes, diagnosis, and remediation of a wide variety of coating defects.

What we shall call "flow defects" represent a local variation in film thickness. They arise from some local nonuniformity affecting the liquid coating layer, such as a gradient in surface tension, causing a surface shear stress that results in a surface flow and bulk flow that ultimately can produce, for example, a crater.[5] Such so-called Marangoni flows can be generated from surface contamination by a low-energy material and also by local disparities in solvent evaporation during film formation.[6] In the latter case, the Marangoni effect has been shown to both initially accelerate leveling and also "overdrive" the leveling process to the point of worsening (coarsening) with a negative impact on leveling.[7,8] Marangoni flows can thus result in a defect in a coating layer on an otherwise uniform substrate. It should perhaps be noted here that any initially uniform liquid coating layer is actually unstable with respect to breakup to droplets the more readily when the liquid forms a larger contact angle on the solid.[9] This is a Rayleigh-type instability, where there is an unstable wavelength at which a disturbance can grow, leading to film breakup (termed reticulation), and has nothing to do with any surface tension gradient mechanism, as would pertain in cratering phenomena.

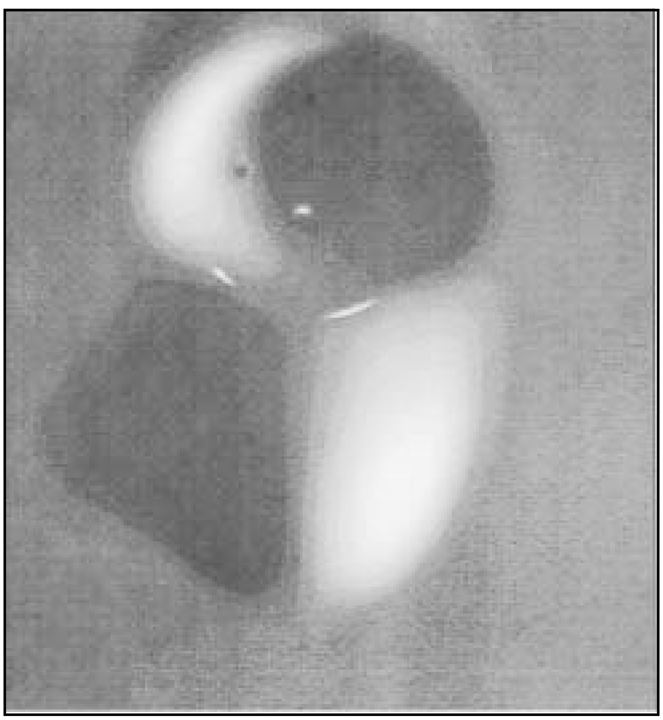

Figure 1—Dripmark defect.

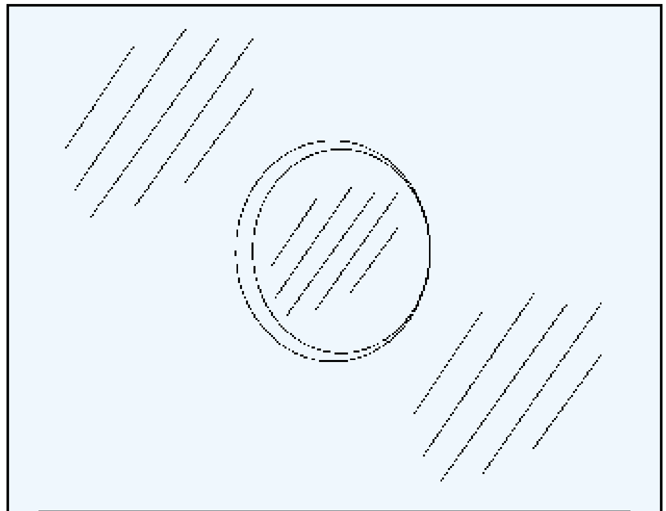

Figure 2—Drawing of a nailhead depression.

Sagging and Dripmark Formation

Coating defects can also occur in situations where the surface tension is uniform, if the substrate geometry is nonuniform or irregular in shape.[9,10] In this case, local variations in curvature (inside and outside corners, sharp edges, or holes), in conjunction with the liquid surface tension, generate capillary pressure gradients that drive the coating to become nonuniform in thickness. In these circumstances, a body force, such as gravity or centrifugal force, acting on the liquid layer can initiate a "fingering flow," leading to a defect sometimes called a "dripmark." A typical example of a dripmark is shown in *Figure* 1. Dripmarks can form in the absence of surface tension gradients, due to a capillary-pressure driven accumulation of liquid on substrates of irregular geometry, such as a mitered corner in a door or window frame. Although dripmark defects are ubiquitous in the architectural coatings industry and in industrial coatings as well, relatively little attention has been given to this particular type of defect in the literature.

On a nonhorizontal substrate, a liquid coating layer will flow or drain downward under the influence of gravity. For a coating on a vertical wall, for example, this is usually called sagging. Sagging is driven by gravitational shear stress σ_g whose magnitude depends on the wet film thickness h and density ρ:

$$\sigma_g = \rho g h \cos\theta \tag{1}$$

(where g is gravitational acceleration and cos θ=1 for a vertical substrate). Predictions of sagging from viscosities measured at an arbitrary shear rate will be misleading because paints can sag at quite different shear rates, depending on the rheology. The proper way to predict relative sagging tendency is to first select the governing viscosity from a plot of viscosity vs. shear stress, rather than shear rate. The sagging shear stress calculated from equation (1) determines the viscosity controlling sagging from the flow curve.

EXPERIMENTAL METHODS

Physical Property Measurements

Rheological Characterization: The paints used in this study were commercial products. The rheological properties in steady shear of the paints were measured on a TA Instruments AR1000-N Stress Rheometer, at 25°C. A 3 cm stainless steel flat disc or "parallel-plate" at a 1000 µm gap was the primary test geometry for the generation of flow curves. The specimen was enclosed by a solvent-trap cover to inhibit drying during the experiment. The test protocol consisted of a one-minute specimen equilibration period after gap closure, followed by a time-based logarithmic ramp of shear stress. Stress was increased over a three-minute "up-ramp" period, then decreased in similar manner for the "down-ramp." Plots of log viscosity (down-ramp data) vs. log shear stress for two architectural paints, "IL," an interior flat latex, and "22," an exterior flat latex, are shown in *Figure* 11.

It is, of course, the rheology of the paint as applied that governs its performance. As an approximation to the as-applied condition of the paint, the "down-curve" rheology data were used. In addition, thixotropic recovery curves were measured in steady shear at various applied shear stresses, and a flow curve was then constructed point-wise from the recovered viscosity value at an arbitrary recovery time, as a function of the stress applied during the recovery phase. This was done in an attempt to take account of the effect of thixotropy during paint drainage. A comment might be made here that if one were concerned with spray-applied coatings, both the composition and the state of dispersion could change as a result of the spraying process. Consequently, rheological characterization should be done on collected sprayed material in that case, with time-dependence as an additional complication.

The AR1000 and other similar instruments can apply a wide range of precise and very stable torques to the specimen, measuring the resulting angular displacement by means of a high-resolution optical encoder. This instrument type is particularly well suited for the characterization of the rheology of complex fluids such as paints, in that the specimen is not forced to flow at a specified shear rate, but rather can be gently "nudged" with increasing force. The material is thereby permitted to display its intrinsic mechanical properties without the premature destruction of the delicate structures responsible for them. It is necessary to accurately measure the viscosity in the very low shear stress range in order to explain sagging and dripmark behavior, as will be shown later.

Surface Tension Measurement

Equilibrium surface tension of the paints was measured using the Wilhelmy balance technique.[11] A cleaned, lightly flamed glass cover slip was used as a probe. A high relative humidity was maintained in the measurement chamber to prevent paint drying on the slide during the measurement.

Density Measurement

Paint density was determined by measuring the weight of a 10 mL syringe containing a measured volume of paint, corrected for the weight of the syringe.

Preparation of Paint Films

Figure 2 shows a drawing of a nailhead depression that can produce the type of dripmark seen in *Figure* 1. In order to simulate the geometry of a countersunk or depressed nailhead, a 10 in. by 8 in. by 3/8 in. aluminum panel was prepared having precision-machined holes of varying depth and width in a two-by-four array. The holes were evenly spaced at 2 in. on-center on the length and 3 in. on-center on the width. In conformity with the "small-slope" approximation inherent in the lubrication theory, the walls of the "nailholes" were machined at a 45° angle, thus softening the radii of curvature at the hole edges or corners. This is not unlike the actual geometry where a nail has been "set" below the surface of a wooden substrate.

The panel was positioned in a vertical orientation for maximum effect of gravitational force on flow. The mounting assembly permitted the easy positioning of the panel so as to present the target hole for a particular experiment. Paints were applied to the vertical aluminum panel using

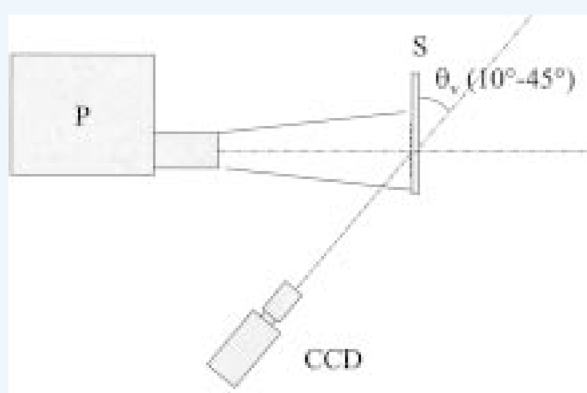

Figure 3—Plan view of projector-CCD camera system.

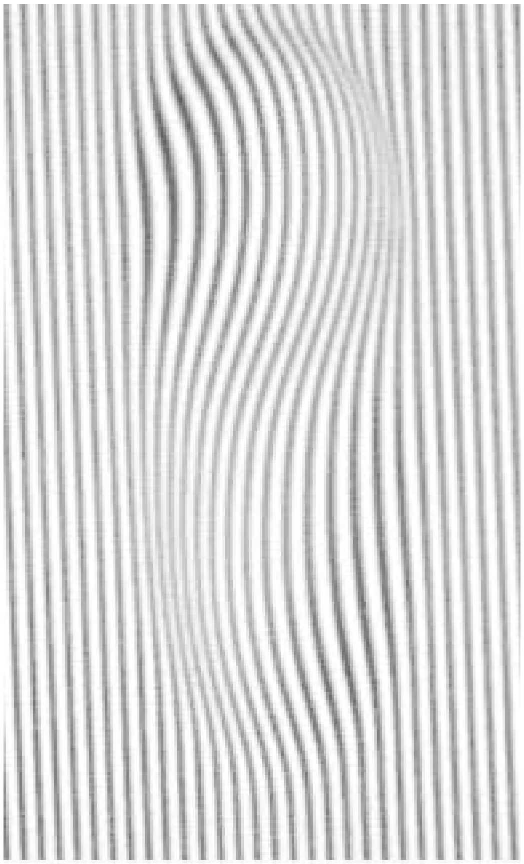

Figure 4—Image of dripmark with projected Ronchi ruling array.

a steel 6 in. wide, nominally 6 mil drawdown bar (Bird blade). Video image capture at a frame rate of two frames/sec was commenced prior to drawdown.

Film laid down by a drawdown bar is thicker when the substrate is oriented vertically than when applied in a horizontal position, due to the lower pressure the operator is able to exert. The hydrodynamic pressure under the bar, a function of the rheology, determines the applied film thickness. Thus, a paint of high viscosity at the shear stresses of drawdown can produce a wet film of up to 9 mils using a 6 mil drawdown bar. Applied film thickness was measured with a precision wet-film gauge shortly after drawdown.

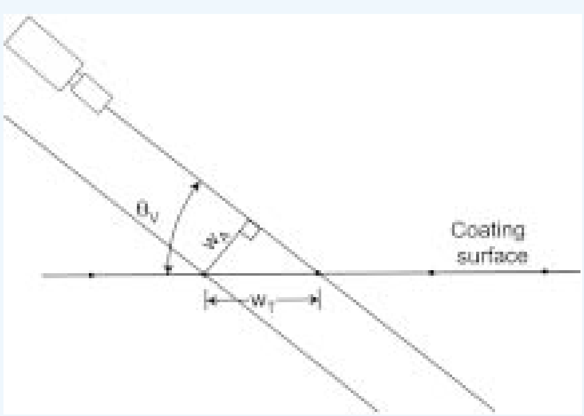

Figure 5—Coating surface with projected line array (dots). θ_V is camera view angle. w_T is the true projected line spacing, w_A the apparent line spacing.

Surface Profile Measurement by Line-Spacing Analysis

In order to compare the results of the computer simulations with experiment, a method was needed to measure the local variation in real time of the coating surface height in the vicinity of a coating defect. The quantitative, time-based, three-dimensional measurement of the variation in height of a coating surface is experimentally somewhat difficult. Existing methods include laser confocal microscopy and optical reflected interferometry,[12] the former involving costly instrumentation and the latter being unavailable commercially.

We report here a new method (to the authors' knowledge) for measuring the surface profile of a coating, by analysis of the apparent line spacing (when viewed obliquely) of a grid or parallel line array projected onto the coating surface. *Figure* 3 shows a schematic arrangement of projector, substrate panel, and camera. The projector *P* is used to form the image of an array of parallel lines or a line grid on the substrate *S*. *Figure* 4 is a dripmark image with a projected parallel line array made using a 150 line-per-inch Ronchi Ruling (projected line density 50 lines/in.). The distorted pattern of projected vertical lines due to the nonuniform liquid surface is visible. The image is approximately 1.5 cm × 0.75 cm.

Since we are studying gravitationally-driven flows, the substrate is a vertically oriented aluminum panel having several precisely machined holes of known width and depth. The video camera is positioned at a known angle with respect to the panel (or the angle can be computed from the image calibration). The live image of the freshly applied paint film on the panel surface is acquired by a charge-coupled device (CCD) camera interfaced with a dedicated frame capture card which converts the video signal from the camera into a digital image. Multiple images may be captured at a specified frame rate, to make a "movie" of the film flow. The sequence of digitized images is stored on the computer hard drive for later analysis.

In *Figure* 5, a flat liquid coating surface (viewed in-plane) is depicted, with dots representing an array of parallel lines projected onto the surface, of true spacing w_T. The camera viewing angle is θ_V. Viewed from θ_V, the apparent line separation is w_A. It is apparent that

$$\sin\theta_V = \frac{w_A}{w_T}. \qquad (2)$$

In *Figure* 6, the projected lines on the substrate are represented as open circular points of spacing w_T. When viewed at an angle $\theta_V<90°$, the apparent line spacing will be w_A for a planar surface, where $w_A<w_T$. If the surface of projection were flat, the spacing apparent to the camera would be w_A. If, however, the surface of projection has a slope such that the projected line intersects the surface at a height incre-

ment Δh_i, then the apparent line spacing from the camera's point of view would be $w_A + d_i$. Away from the indentation and the liquid surface irregularity, the surface is essentially flat and this region provides a set of reference straight (undistorted) lines. Relative to the reference straight line, a set of values of d_i gives the shape of a vertical section through the liquid. From *Figure* 6,

$$\cos\theta_V = \frac{d_i}{\Delta h_i}. \quad (3)$$

Figure 7 is another dripmark image with projected ruling lines. The edge of the circular indentation underlying the paint layer is outlined. Also shown are a vertical straight line connecting undistorted ruling lines (reference line) and a curved line following one of the distorted rulings. The difference between the latter two lines is the apparent surface height or depth. The shape of the distorted vertical line is actually a vertical cross section of the free surface, scaled by the cosine of the camera viewing angle θ_V. To convert the apparent depth or height of this vertical cross section to the actual value Δh_i, from equation (3),

$$\Delta h_i = \frac{d_i}{\cos\theta_V}. \quad (4)$$

The cumulative surface profile is obtained by summing the local Δh_i values:

$$h_j = \sum_{i=l}^{j} \Delta h_i = \frac{1}{\cos\theta_v} \sum_{i=l}^{j} d_i. \quad (5)$$

When the above calculations and corrections are performed, conveniently in a spreadsheet, a three-dimensional map of the coating defect may be generated, as shown in *Figure* 8. *Figure* 8 is a ribbon-plot of the surface height (mm) against the coordinate in the direction of gravity (mm) for an array of image lines. Such data may be smoothed and used to produce rotatable 3-D views such as those in *Figure* 9. This process is somewhat laborious, but by using computerized image analysis, the process can be computer automated. The foregoing derivation assumes the camera to be located at infinity, so that the lines of sight are parallel. In practice, however, a geometric correction for parallax must be applied to the measured line spacing, without which the calculation would show a systematic error, where the relative surface height in the flat areas would not return to zero on the far side of the plot.

MATHEMATICAL MODEL AND NUMERICAL SIMULATION METHOD

Although it is possible that certain coating application processes involve turbulent or three-dimensional flow (e.g., spray application and industrial rollcoating), once a thin fluid film has been laid down the subsequent flow is predominantly laminar and fairly slow. This being the case, the application of the so-called *lubrication approximation*, a simplified form of the Navier-Stokes equations for fluid flow, is justified to describe coating flow in such a fluid layer. In the lubrication model, properties are integrated across the thin dimension, hence averaged in the direction normal to the coating layer. This simplified equation set reduces the computational load by several orders of magnitude, and has been shown in most cases to give answers within a few percent of the non-approximate

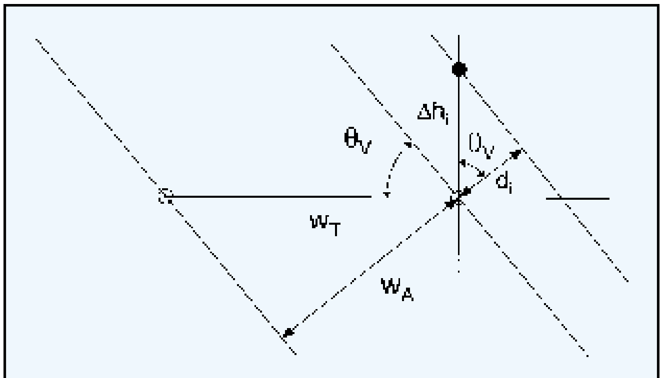

Figure 6—Defining geometric relationships for line-spacing analysis.

Figure 7—Dripmark with projected Ronchi ruling. The rim of the circular indentation underlying the paint layer is outlined. Also shown are a vertical straight line connecting undistorted ruling lines (reference line) and a curved line following one of the distorted rulings. The difference between the latter two lines is the apparent surface height or depth.

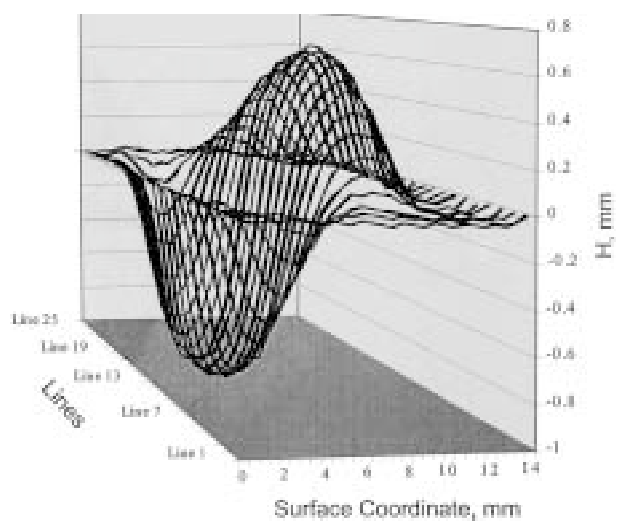

Figure 8—Ribbon plot from line-spacing analysis, representing the surface height H (mm) vs. surface coordinate (mm) in gravitational direction.

solution. Furthermore, this approach enables the solving of problems of otherwise intractable complexity. We present a mathematical approach based on the lubrication model that leads to an evolution equation for the liquid layer thickness variation. Finite difference methods are used for solving the equation. Results from some unsteady flow calculations are shown.

We use a right-handed three-dimensional Cartesian coordinate system with the (x,y) plane lying on the flat or "land" area of the substrate. The x axis is directed vertically downward and z is the distance measured perpendicular to the substrate. At any instant of time, the free surface of the coating is given by the function $z=h(x,y,t)$ where t is time. The liquid layer is bounded above by a stress-free surface upon which surface tension acts. The layer is bounded below by the substrate whose equation is $z=h_1(x,y)$. Thus, the thickness of the coating is given by $h-h_1$. Here h_1 is taken to be the equation of a circular indentation with a flat bottom, corresponding, for example, to a nail head that has been "set" using a punch (see *Figure* 2). The evolution equation for the free surface shape follows from application of the global mass conservation equation

$$\frac{\partial h}{\partial t} = -\nabla \cdot \mathrm{Q} \cdot \qquad (6)$$

Here, ∇ is the two-dimensional differential operator with respect to the orthogonal substrate coordinates x and y. **Q** is the flux vector defined by

$$\mathrm{Q} = \int_{h_1}^{h} \mathrm{u}\, dz \qquad (7)$$

where **u** is the vector velocity. The vector **u** is essentially parallel to the flat substrate. Kim et al.[13] used this approximate treatment for Newtonian flow over roughened substrates.

Non-Newtonian rheology can be included via a non-Newtonian constitutive relation such as the Ellis model. According to this model (Bird, et al.[14]), the viscosity η depends on the stress σ according to,

$$\eta = \frac{\eta_0}{\left(1 + \left|\frac{\sigma}{\sigma_{1/2}}\right|^{\alpha-1}\right)}. \qquad (8)$$

Here the parameter $\sigma_{1/2}$ is the value of shear stress at which the viscosity is equal to one-half the zero-stress Newtonian value η_0. The degree of shear thinning is controlled by the exponent α; $\alpha = 1$ corresponds to Newtonian flow and $\alpha > 1$ to shear-thinning behavior. The Ellis model is a typical generalized-Newtonian flow law; other constitutive relations can also be implemented.

We apply the no-slip condition on the substrate and the condition $\sigma = 0$ on $z = h$. The constitutive law $\sigma = \eta u_z$ (where the subscript z denotes differentiation of the velocity with respect to the normal coordinate) can be integrated to find the velocity profile across the thin dimension of the liquid layer. The result, for the flux, is

$$\mathrm{Q} = -\frac{\nabla p}{3\eta_0}(h-h_1)^3\left[1+\left(\frac{3}{\alpha+2}\right)\left(\frac{|\nabla p|(h-h_1)}{\sigma_{1/2}}\right)^{\alpha-1}\right]. \qquad (9)$$

Here the pressure gradient has contributions from capillary pressure (surface tension) and gravity, the latter acting in the positive x direction. The unit vector in the x-direction is **i**. Thus

$$\nabla p = -\gamma \nabla \nabla^2 h + \rho g \mathrm{i} \qquad (10)$$

where γ is surface tension, ρ the liquid density, and g gravitational acceleration.

Weidner and Schwartz reported a model for gravity drainage flow in one space dimension using the Ellis model.[15] Three-dimensional drainage flow from gravure

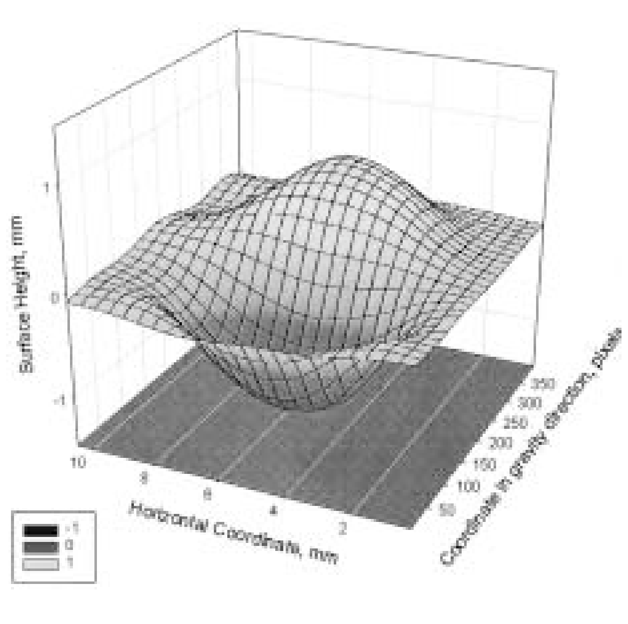

Figure 9—Smoothed surface plot of surface height data from line-spacing analysis.

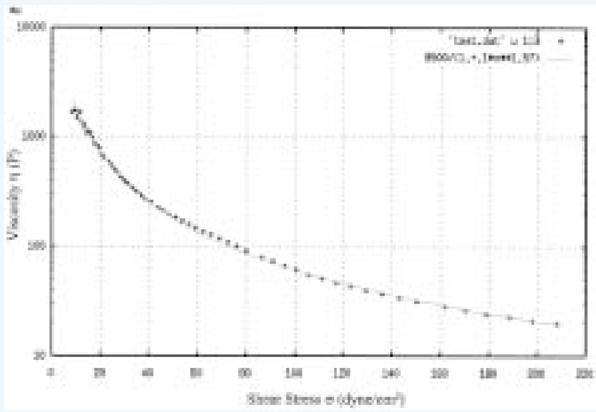

Figure 10—Ellis model fit of flow curve data for paint "22."

cells was simulated by Schwartz et al.[16] A general survey of modeling techniques for thin-layer free-surface flows is given in Schwartz.[17]

It is useful, for computational purposes, to write the evolution equation in dimensionless variables. In this technique, variables of length and time are scaled by reference values which are characteristic of the system geometry and physical properties. The equation becomes

$$\frac{\partial h}{\partial t} = -\frac{\partial s}{\partial t} - \nabla \cdot \left(s \nabla \nabla^2 h\right). \tag{11}$$

Here s is the "permeability," taking into account the thinning behavior. Specifically,

$$s = \left(h - h_1\right)^3 F \tag{12}$$

where F is the factor in square brackets in equation (9), or, more generally, is the function determined from the rheological data, or flow curve. It may be helpful here to point out certain analogies between fluid mechanics and the flow of electricity. For example, the electrical analogue of the voltage driving the flow of electrical current is a pressure gradient. The fluid flux Q resulting from a pressure gradient is analogous to the current I, and the "permeability" s in fluid mechanics is like the conductivity, i.e., how easily electrons can move through a conductor. Equation (12) states that the permeability s or fluid "flowability" is proportional to the cube of the local film thickness. This relationship has its counterpart in the well known Orchard equation[18] for the leveling of a viscous fluid, in which the rate of decay of sinusoidal variations in liquid layer thickness is proportional to h^3. In equation (12), the thickness is now written as a multiple of h_0, the initial uniform coating thickness on the "land" or flat areas of the substrate. This is the unit of length in the z direction.

Table 1—Example Parameter Values for Simulation

36.5	Surface tension (dyne/cm)
1.34	Liquid density (g/cm^3)
0.0216	h_0, land coating thickness (cm)
0.714	Indentation diameter (cm)
0.0762	Indentation depth (cm)
2.6	Ellis α
0.08	Ellis $(\sigma_{1/2})^{-1}$
190	Viscosity (poise) at stress = 50 dyn/cm^2

For the substrate coordinates (x, y), the dimensionless length unit is

$$L_1 = \left(\frac{\gamma h_0}{\rho g}\right)^{1/3}. \tag{13}$$

The reference time is

$$T_1^* = \frac{3\eta_0 L_1}{\rho g h_0^2} \tag{14}$$

where the reference viscosity is $\eta_0 = \eta(\sigma_0)$ and $\sigma_0 = \rho g h_0$, the gravitational shear stress level for the initial uniform coating. Given the configuration of the initial coating, equation (11) is used to predict its subsequent flow behavior.

The dimensionless equation (11) is solved by a finite difference method in space and time. The substrate is discretized into an $M \times N$ rectangular computational domain. Spatial derivatives are approximated using central differences; thus, the method is second-order accurate in space. Time marching is made efficient using a novel semi-implicit method. It is similar, in principle, to alternating direction (ADI) methods used for second-order diffusive problems, as discussed by Peaceman.[19] Nonlinear prefactors in s are evaluated at the "old" time level. Thus, the method is only first-order accurate in time. However, convergence is easily verified under temporal refinement and time steps are adjusted accordingly. Because of the severe stability requirements for an explicit solution, for which the time step Δt is restricted to being smaller, in an order-of-magnitude sense, than the fourth power of the space step Δx, i.e.,

$$\Delta t < O(\Delta x)^4, \tag{15}$$

the present implicit method is faster by several orders of magnitude compared to an explicit scheme. The method is also much faster than time integration if the ADI technique were not used, in which case very large banded

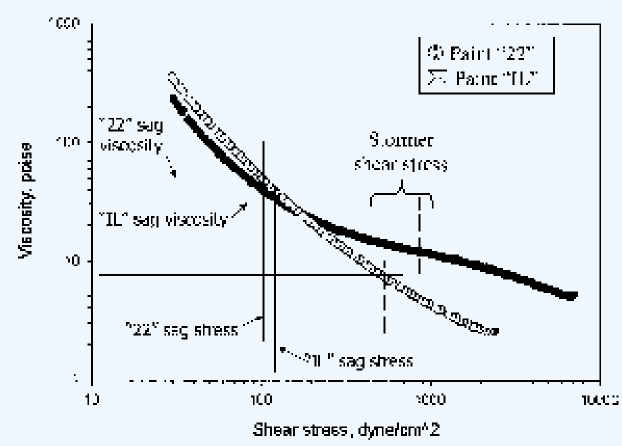

Figure 11—Viscosity vs. shear stress curves for paints "IL" and "22." Approximate Stormer shear stresses are indicated by the dashed lines. Also shown are the sagging shear stresses for the two paints, calculated from the maximum paint layer thickness obtained from the computer simulation and the corresponding paint viscosities governing the drainage flow.

Table 2

	Stormer Viscosity, KU	"ICI" Viscosity, Poise
Paint "IL"	125	1.6
Paint "22"	107	1.0

systems of equations would have had to be solved. For a given simulation, computer usage is proportional to the number *MN* of calculated *h* values. Ten thousand or more *h* values are used. Typical calculations require a few minutes on a PC with an Athlon 1200 processor, using the public domain Linux operating system.

The rheology of the paint can be introduced into the simulation via a mathematical model relating viscosity and shear stress. The Ellis model was chosen for this work (equation (8)). *Figure* 10 shows the fit of the Ellis model to the experimental flow curve in the region of sagging shear stresses, for paint "22." Typical parameter values for a simulation are shown in *Table* 1.

It was found, however, that experimental paint flow data do not conform well to standard constitutive models such as the Ellis equation, as a general rule. Consequently, a method was developed for utilizing measured rheological data directly via a look-up table and computing from it an effective local fluidity. For details of the method, see Schwartz and Eley.[20] Use of viscosity-shear stress data directly permits flow curves of complex shape (not an unusual occurrence for paints) to be analyzed.

DISCUSSION

Role of Rheology in Sagging Flow

Before discussing the manner in which coating rheology controls application and leveling, as well as undesirable flows leading to film defects (e.g., sagging, cratering, crawling, edge withdrawal), there is an important initial point to be made. Such flows are driven by specific shear stresses, which can be calculated from the forces acting (e.g., gravity and surface tension) and the geometry of the film and substrate.[21,22] However, these flow processes can occur over a wide range of shear rates, depending on the coating viscosity at the acting shear stress. The shear *stress* acting on a coating layer (for a given process) is *independent* of the rheology. In contrast, the shear *rate* will be *dependent* on paint rheology. Comparison of paint viscosities as a function of shear rate will often be misleading. It is preferable to represent flow data as viscosity vs. *shear stress* plots, as opposed to viscosity vs. *shear rate*, which is the more common practice. The shear rate is a dependent variable, for real processes. For several reasons, the appropriate independent variable for evaluating and differentiating the performance of paints according to their rheology is the shear stress.[22]

The flow curves of paints "IL" and "22" are shown in *Figure* 11 as a double-logarithmic plot of viscosity vs. shear stress. The "down" curve data are shown and were used for calculation purposes, since the majority of the drainage flow takes place immediately after the paint has been sheared at 500-800 sec^{-1} during drawdown. In reality, there is some time dependence in the two paints, and the thixotropic nature of the paint should be accounted for in the mathematical model. This is an intended next step in the work.

It can be seen in *Figure* 11 that "IL" is at first lower than "22" (at low shear stresses), then crosses over "22" at around 150 dyne/cm^2, and is several times higher in viscosity at higher shear stresses. In fact, "IL" feels definitely thicker than "22" if stirred by hand, a fact that is reflected in the higher Stormer viscosity of "IL" (125 KU vs. 107 KU for "22"). (See *Table* 2.)

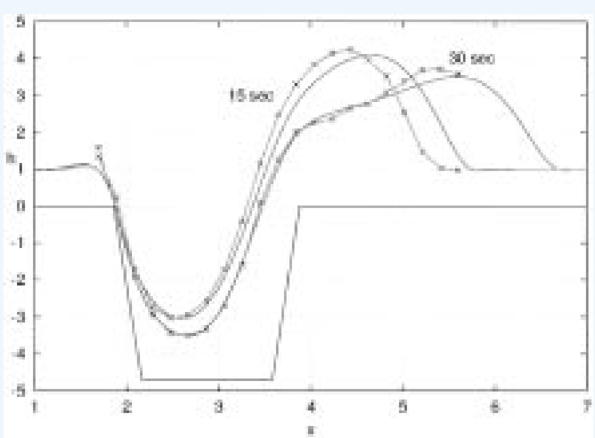

Figure 12—Comparison of theoretical and experimental centerline plots for paint "IL." Solid curve is simulation; x is experiment. The "nailhead indentation" and substrate surface are shown underlying the paint surface profiles. In the figures, the vertical axis is h/h_0, the film height normalized to the applied film thickness. The horizontal axis is in units of the "nailhole" radius.

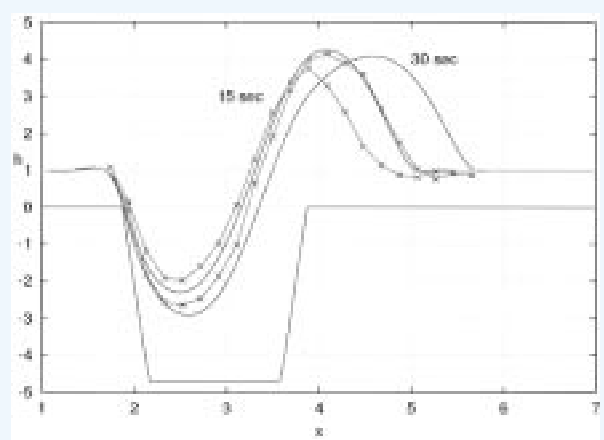

Figure 13—Comparison of theoretical and experimental centerline profiles for paint "22." Solid curve is simulation; x is experiment. The "nailhead indentation" and substrate surface are shown underlying the paint surface profiles. In the figures, the vertical axis is h/h_0, the film height normalized to the applied film thickness. The horizontal axis is in units of the "nailhole" radius.

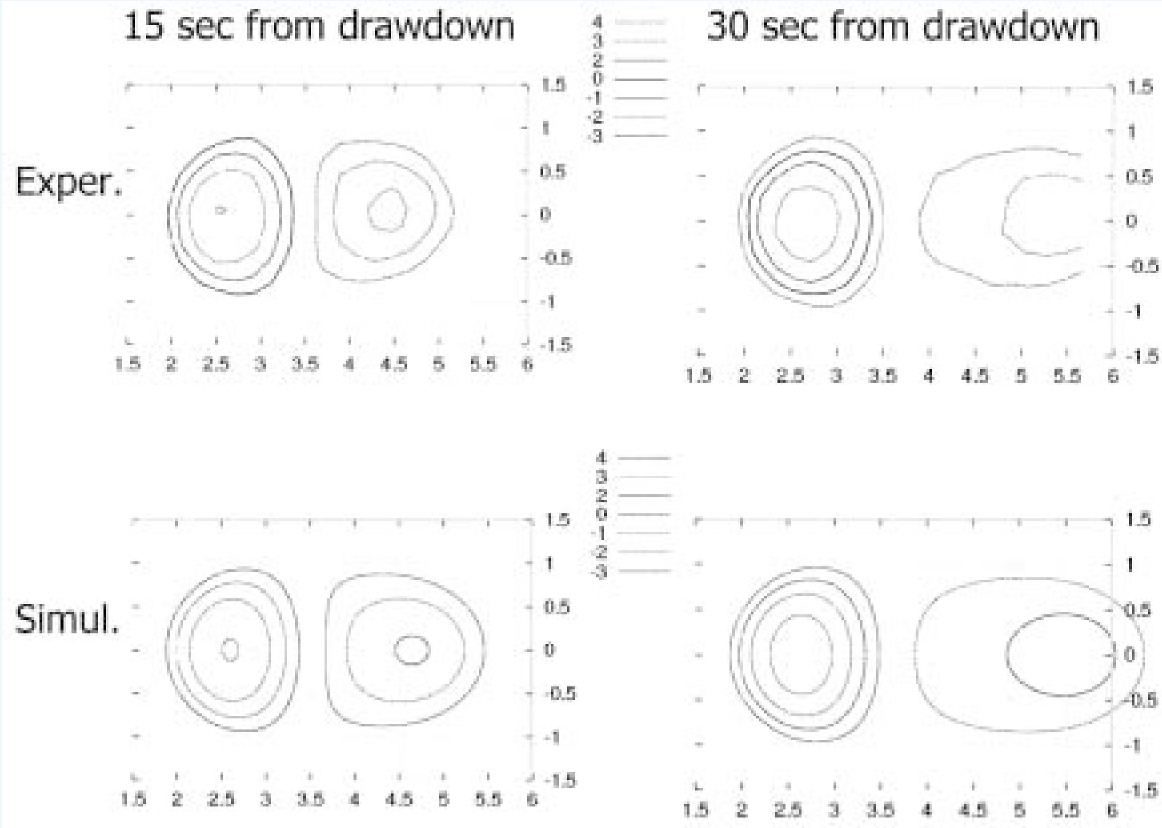

Figure 14—Comparison theoretical and experimental contour plots for paint "IL." Top row of figures is from experiment and bottom row from the simulation. Left column of images is 15 sec from drawdown, right column is 30 sec from drawdown.

In *Figure* 11, the approximate Stormer shear stress is indicated by a heavy dashed line (calculated assuming a Stormer shear rate of about 70 sec^{-1}). If one were to infer the relative sagging and dripmark tendencies from the KU viscosities, one would predict the opposite of what is observed. The reason for this paradox is that sagging stresses are in a very different range from those in a Stormer measurement. The maximum shear stress acting on the dripmark was calculated from the measured maximum film height taken from "centerline plots" (*Figures* 12 and 13), which were obtained by line-spacing analysis. Thus, for paint "IL" at 15 sec from drawdown, the maximum film thickness is 4.2 h_0 or 0.93 mm (h_0, the applied wet film thickness = 0.22 mm). Similarly for paint "22" the film height at the thickest point of the dripmark is 3.7 h_0, or 0.80 mm. From these numbers and the wet density, the shear stress driving drainage is calculated from equation (1) to be 122 dyne/cm^2 for "IL" and 105 dyne/cm^2 for "22." From the flow curve, one then obtains that the viscosity controlling the sagging velocity is 32 P for "IL" and 47 P for "22." These sagging shear stresses and viscosities are indicated on *Figure* 11. While "sagging viscosities" are quoted here, it should be remembered that as the gravitational shear stress is a maximum at the substrate and zero at the free surface, so the viscosity varies (nonlinearly) through the film from a minimum at the substrate to a maximum at the free surface. Consequently, and for reasons of other complexities, the true gravitational drainage flux must be calculated by numerical simulation. Nevertheless, it is useful to apply these principles, together with flow curve analysis, to gain a better understanding of the sagging and dripmark formation behavior of paints and coatings.

Comparison of Simulation and Experiment

Figures 12 and 13 show "centerline profile" comparisons of theoretical prediction and experiment for paint "IL" and paint "22," respectively. Drainage profiles are shown at 15 and 30 sec after drawdown. The substrate and its indentation are shown underlying the surface profile curves. The agreement of model and experiment is quite close for "IL," but in actuality the coating drains somewhat less rapidly for "22" than the model predicts. The prediction of the surface profile and thickness inside the "nailhead depression" itself is quite good. The model shows, in agreement with the experiment, that the coating becomes very thin near the upper edge of the nailhole, but that the extent of thinning at the base of the depression, and thus the ability to fill a substrate defect, is dependent on rheology. The slight under-prediction of coating thickness above the nailhole is easily accounted for, as follows. The simulation did not include drainage of paint from the regions far above the depression, whereas in reality this

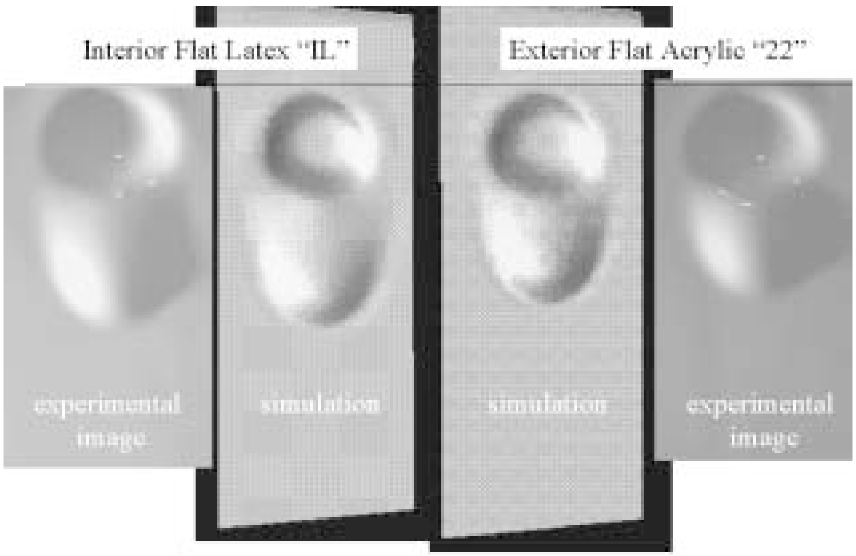

Figure 15—Comparison of experimental and simulation dripmark images at 15 seconds after drawdown. Paint "IL" images on left and Paint "22" images on right.

cumulative drainage will result in a "pileup" of fluid at the upper rim of the depression, shown by the experimental data, particularly in *Figure* 12. (The excess fluid is largely prevented by surface tension from flowing past the small radius at the rim into the depression.)

Figure 14 shows contours of constant surface height for Paint "IL" at 15 and 30 sec from drawdown. The x and y axes are in units normalized to the radius of the nailhole and the scale for the contours in the figure legend is in units of h_0, the applied wet film thickness. In each figure the nailhole (depression) is on the left and the dripmark (bump) is on the right. The top row of figures represents experimental data from line-spacing analysis and the bottom row is from the computer simulation. The similarity between the experiment and the simulation is even more evident in these three-dimensional comparisons than in the two-dimensional plots of *Figures* 12 and 13.

Figure 15 compares experimental photographs with simulation images for "IL," an interior flat latex paint, and "22," an exterior flat acrylic. The images correspond to a 15 sec period from drawdown application. *Figure* 16 shows a similar comparison for the paints at 30 sec after drawdown. The dripmark length ratios of "IL" and "22" from the simulation and the experiment were calculated and compared. It was found from the experiment that the "22" drip length was 72% of the "IL" length, while from the simulation the drip length of "22" was 74% that of "IL." The simulation thus confirms the experimental observation that "IL" sags faster than "22," and by the correct ratio of sag length.

The important thing to note in *Figures* 15 and 16 is not that there are relatively small differences between the two paints' sagging behavior, but rather that such small but real differences in flow behavior can be accurately predicted for two paints of complex rheology by use of very low stress rheological data and a model built from first principles. Noteworthy also is that one would have predicted the opposite sagging result from the usual information, i.e., the Stormer viscosity, the "ICI" viscosity, or even the stirring "feel." Measurement of the viscosities at an arbitrary shear rate of, say, 1 sec^{-1} would have similarly been misleading. Crossover rheological behavior is very common among paints and can lead just as often to a failure of lab-bench measures of rheology to correlate to paint performance.

Some other features common to simulation and experiment are worthy of comment. The dripmark images in *Figures* 15 and 16 are illuminated from the left. (The three-dimensional representations of the computer images with illumination are done using public-domain software called GEOMVIEW.) There is a pronounced liquid ridge surmounting the nailhole in both the experimental photographs and the computer-generated images, evidenced by the shadow it casts to the right of the hole. This ridge

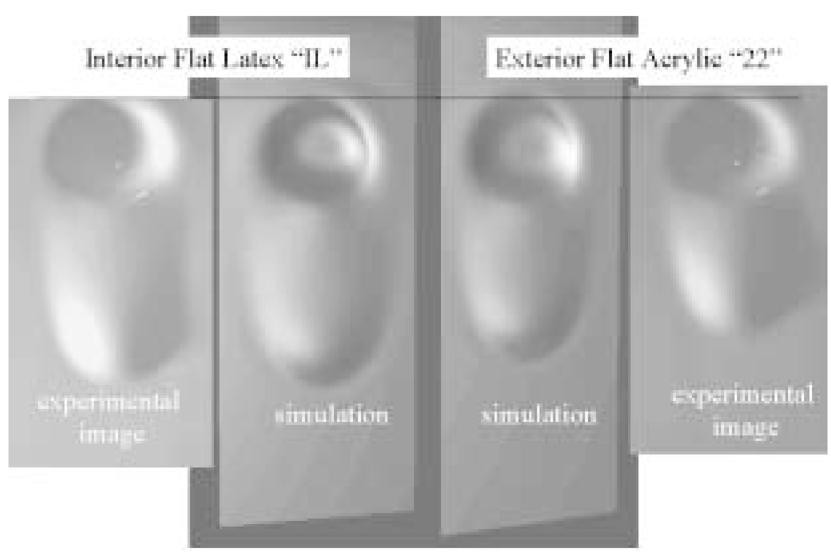

Figure 16—Comparison of experimental and simulation dripmark images at 30 seconds after drawdown. Paint "IL" images on left and Paint "22" images on right.

develops early in the flow and is readily explained. Surface tension combined with the small radius of curvature of liquid initially covering the edge causes the pressure at the edge of the hole to increase. Because this edge is relatively sharp, the pressure is large there and drives the liquid away. The coating becomes quite thin at the edge, essentially preventing further flow into the indentation from above. The draining liquid piles up above the edge, but finds a path downward by following a capillary "channel" along the curving edge. The result is a liquid ridge or ring around the indentation. In decorative applications, this will be likely to emphasize an already unsightly defect.

CONCLUSIONS

It was shown that a paint with a higher Stormer viscosity, higher "ICI" viscosity, and a more viscous "feel" can still show worse sagging than a paint of apparently lower viscosity. This behavior can be explained by accurate low-shear-stress viscosity measurements. Results of a theoretical model and numerical simulation of three-dimensional, time-dependent coating flow and dripmark formation have been confirmed by experiment. A novel method for experimental measurement of the evolving surface profile of an opaque, flowing liquid coating, in three dimensions and with high resolution, has been developed. We conclude that numerical simulation together with line-spacing analysis represent powerful tools for the detailed investigation of paint flow defects—tools that are capable of defining with great precision the interrelated roles of rheology, substrate geometry, and process variables in determining coating outcomes.

ACKNOWLEDGMENTS

We gratefully acknowledge the experimental assistance of Ms. Kimberly Hennigan, Ms. Pamela Kuschnir, and Mr. Stefan Posakiwsky. We thank ICI Paints for permission to publish.

References

(1) Strivens, T.A., "The Rheology of Paints," in *Paint and Surface Coatings: Theory and Practice*, Lambourne, R. and Strivens, T.A. (Eds.), 2nd ed., Woodhead Pub. Ltd., 1999.

(2) Schoff, C.K., "Surface Defects: Diagnosis and Cure," Journal of Coatings Technology, *71*, No. 888, 56 (1999).

(3) Pierce, P.E. and Schoff, C.K., "Coating Film Defects," 2nd Edition, *Federation Series on Coatings Technology*, Blue Bell, PA, 1994.

(4) Kornum, L.O. and Raaschou-Nielsen, H.K., "Surface Defects in Drying Paint Films," *Prog. Org. Coat.*, 8, 275 (1980).

(5) Bierwagen, G.P., "Surface Defects and Surface Flows in Coatings," *Prog. Org. Coat.*, 19 (1), 59 (1991).

(6) Weidner, D.E., Schwartz, L.W., and Eley, R.R., "Role of Surface Tension Gradients in Correcting Coating Defects in Corners," *J. Coll. & Interf. Sci.*, 179, 66-75 (1996).

(7) Overdiep, W.S., "The Leveling of Paints," *Prog. Org. Coat.*, 14, 159 (1986).

(8) Wilson, S.K., "The Derivation and Analysis of a Model of the Drying Process of a Paint Film," *Surf. Coat. Int.*, 4, 162 (1997).

(9) Schwartz, L.W., Roy, R.V., Eley, R.R., and Petrash, S., "Dewetting Patterns in a Drying Liquid Film," *J. Coll. Interf. Sci.*, 234, 363-374 (2001).

(10) Hoeflaak, M., "Edge Coverage and Rheological Behaviour of Coating Materials During Film Formation," *Surf. Coatings Australia*, 6, July 1987.

(11) Bierwagen, G.P., "Surface Energetics," Chap. 5.4 in *ASTM Paint and Coatings Testing Manual*, 14th ed., Koleske, J. (Ed.), American Society for Testing and Materials (ASTM), West Conshohocken, PA, pp. 369-382, 1995.

(12) Klarskov, M., Jakobsen, J., and Saarnak, A., "Verification of the Orchard Leveling Analysis," *Rheology*, 92, *30*, March (1992).

(13) Kim, J.S., Kim, S., and Ma, F., *J. Appl. Phys.*, *73*, 422-428 (1993).

(14) Bird, R.B., Armstrong, R.C., and Hassager, O., *Dynamics of Polymeric Liquids*, Wiley, New York, 1977.

(15) Schwartz, L.W., Moussalli, P., Campbell, P., and Eley, R.R., *Trans. Inst. Chem. Engrs.*, 76, 22-29 (1998).

(16) Weidner, D.E. and Schwartz, L.W., "Contact Line Motion of Shear-Thinning Fluids," *Phys. Fluids*, 6 (11), 3535-3538 (1994).

(17) Schwartz, L.W. "Unsteady Simulation of Viscous Thin-Layer Flows," in *Free-Surface Flows with Viscosity*, Tyvand, P. (Ed.), pp. 203-233, Computational Mech. Publ., Southampton, 1997.

(18) Orchard, S.E., *Applied Scientific Research, Section A*, Vol. 11, 451, 1962.

(19) Peaceman, D. *Fundamentals of Numerical Reservoir Simulation*, Elsevier, Amsterdam, 1977.

(20) Schwartz, L.W. and Eley, R.R., "Flow of Architectural Coatings on Complex Surfaces; Theory and Experiment," *J. Eng. Math.* (2002), in press.

(21) Eley, R.R., "Rheology and Viscometry," Chap. 33, *ASTM Paint and Coatings Testing Manual*, 14th ed., ASTM, Philadelphia, 333-368, 1995.

(22) Eley, R.R., "Principles and Methods of Rheology in Coatings," in *Encyclopedia of Analytical Chemistry: Instrumentation and Applications*, Meyers, R.A. (Ed.), J. Wiley & Sons, Ltd., 2001.